Ristretto MRE: A generalized multi-shot GRE-MRE sequence

Guenthner, Christian ; Sethi, Sweta ; Troelstra, Marian ; Dokumaci, Ayse Sila ; Sinkus, Ralph ; Kozerke, Sebastian

Abstract: In order to acquire consistent k-space data in MR elastography, a fixed temporal relationship between the MRI sequence and the underlying period of the wave needs to be ensured. To this end, conventional GRE-MRE enforces synchronization through repeated triggering of the transducer and forcing the sequence repetition time to be equal to an integer multiple of the wave period. For wave frequencies below 100 Hz, however, this leads to prolonged acquisition times, as the repetition time scales inversely with frequency. A previously developed multi-shot approach (eXpresso MRE) to multi-slice GRE-MRE tackles this issue by acquiring an integer number of slices per wave period, which allows acquisition to be accelerated in typical scenarios by a factor of two or three. In this work, it is demonstrated that the constraints imposed by the eXpresso scheme are overly restrictive. We propose a generalization of the sequence in three steps by incorporating sequence delays into imaging shots and allowing for interleaved wave-phase acquisition. The Ristretto scheme is compared in terms of imaging shot and total scan duration relative to eXpresso and conventional GRE-MRE and is validated in three different phantom studies. First, the agreement of measured displacement fields in different stages of the sequence generalization is shown. Second, performance is compared for 25, 36, 40, and 60 Hz actuation frequencies. Third, the performance is assessed for the acquisition of different numbers of slices (13 to 17). In vivo feasibility is demonstrated in the liver and the breast. Here, Ristretto is compared with an optimized eXpresso sequence, leading to scan accelerations of 15% and 5%, respectively, without compromising displacement field and stiffness estimates in general. The Ristretto concept allows us to choose imaging shot durations on a fine grid independent of the number of slices and the wave frequency, permitting 2- to 4.5-fold acceleration of conventional GRE-MRE acquisitions.

DOI: https://doi.org/10.1002/nbm.4049

DOI: https://doi.org/10.1002/nbm.4049

Received: 9 May 2018 | Revised: 16 October 2018 | Accepted: 9 November 2018

DOI: 10.1002/nbm.4049

RESEARCH ARTICLE

WILEY NMR IN BIOMEDICINE

Ristretto MRE: A generalized multi-shot GRE-MRE sequence

Christian Guenthner[1] | Sweta Sethi[2] | Marian Troelstra[3,4] | Ayse Sila Dokumaci[3] | Ralph Sinkus[3] | Sebastian Kozerke[1]

[1] Institute for Biomedical Engineering, University and ETH Zurich, Zurich, Switzerland

[2] Division of Research Oncology, Guy's and St Thomas' NHS Foundation Trust, London, UK

[3] Division of Imaging Sciences & Biomedical Engineering, King's College London, London, UK

[4] Department of Radiology and Nuclear Medicine, Academic Medical Center, Amsterdam, The Netherlands

Correspondence
C. Guenthner, Institute for Biomedical Engineering, University and ETH Zurich, Zurich, Switzerland.
Email: guenthner@biomed.ee.ethz.ch

Funding information
Horizon 2020 Framework Programme, Grant/Award Number: 668039

In order to acquire consistent *k*-space data in MR elastography, a fixed temporal relationship between the MRI sequence and the underlying period of the wave needs to be ensured. To this end, conventional GRE-MRE enforces synchronization through repeated triggering of the transducer and forcing the sequence repetition time to be equal to an integer multiple of the wave period. For wave frequencies below 100 Hz, however, this leads to prolonged acquisition times, as the repetition time scales inversely with frequency. A previously developed multi-shot approach (eXpresso MRE) to multi-slice GRE-MRE tackles this issue by acquiring an integer number of slices per wave period, which allows acquisition to be accelerated in typical scenarios by a factor of two or three. In this work, it is demonstrated that the constraints imposed by the eXpresso scheme are overly restrictive. We propose a generalization of the sequence in three steps by incorporating sequence delays into imaging shots and allowing for interleaved wave-phase acquisition. The Ristretto scheme is compared in terms of imaging shot and total scan duration relative to eXpresso and conventional GRE-MRE and is validated in three different phantom studies. First, the agreement of measured displacement fields in different stages of the sequence generalization is shown. Second, performance is compared for 25, 36, 40, and 60 Hz actuation frequencies. Third, the performance is assessed for the acquisition of different numbers of slices (13 to 17). In vivo feasibility is demonstrated in the liver and the breast. Here, Ristretto is compared with an optimized eXpresso sequence, leading to scan accelerations of 15% and 5%, respectively, without compromising displacement field and stiffness estimates in general. The Ristretto concept allows us to choose imaging shot durations on a fine grid independent of the number of slices and the wave frequency, permitting 2- to 4.5-fold acceleration of conventional GRE-MRE acquisitions.

KEYWORDS

eXpresso, GRE-MRE, interleaved acquisition, MR elastography, multi-shot, multi-slice

Abbreviations used: BH, breath hold; FOV, field of view; GRE, gradient-recalled echo; MEG, motion encoding gradient; MRE, magnetic resonance elastography; RMSE, root-mean-square error; SE, spin-echo; SNR, signal-to-noise ratio; TTL, transistor-transistor logic

Symbols used: $\Delta\varphi$, per-slice reference phase offset; GCD(·, ·), greatest common divisor; k_y, e, phase encode line, motion encoding direction; LCM(·, ·), least common multiple; N_P, φ_p, p_n, number of mechanical phase offsets, phase-offset, phase-offset index; N_S, s_d, i_d, number of slices, slice, index of slice in multi-slice train; N_{SPP}, slices per wave period (eXpresso); N_W, N_D, number of waves, delay (Ristretto); $\vec{r}$, θ, wave displacement, phase; T, f, mf, wave period, frequency, harmonics; T_{IS}, T_R, imaging shot duration, per-slice repetition time; $\vec{x}$, spatial coordinate

1 | INTRODUCTION

Magnetic resonance elastography (MRE) utilizes phase-contrast sequences to measure the three-dimensional shear wave displacement field generated by a synchronized external transducer.[1] The subsequent application of a wave-inversion algorithm allows for the determination of the underlying tissue biomechanics.[2] The technique can be applied to non-invasively assess chronic liver diseases,[2-11] probe breast[12,13] and brain[14-20] tumors, and shows promising results in e.g. the prostate.[21-24]

Key to successful deployment of MRE for research and clinical applications is the reduction of scan time. While new encoding concepts such as sample interval modulation,[25] selective spectral displacement projection,[26] or multi-directional reduced motion encoding[27] show promising scan time reductions for spin-echo (SE)-based MRE sequences, these concepts cannot be readily transferred to gradient-recalled echo (GRE)-based MRE, where imaging gradient contributions need to be corrected for.[28] While SE-based MRE can utilize full wave encoding and typically relies on EPI readouts for fast MRE acquisition, GRE-based MRE needs to balance signal loss due to T_2^* decay and motion sensitivity through fractional encoding.[29,30] To this end, multi-slice GRE-MRE has become the standard in volumetric GRE-MRE, where the interleaved excitation of slices allows the per-slice repetition time to be maximized to reduce partial saturation effects, increasing signal-to-noise ratio (SNR). In conventional GRE-MRE, imaging shot durations are forced to be an integer multiple of the wave period to ensure *k*-space consistency, while the wave-phase offsets are obtained through temporal shifting of the trigger with respect to the MRI sequence.[1,31] Thus, at wave frequencies below 100 Hz, acquisition duration typically becomes prolonged. In order to reduce the scan duration, Garteiser et al proposed eXpresso MRE, a multi-shot sequence with fractional encoding that allows multiple slices to be acquired per wave period.[30] Sequence delays are used to shift the multi-slice acquisition train with respect to the wave period to allow for the successive acquisition of the wave-phase offsets. While the concept allows suitable sequence parameter combinations, which minimize the scan duration, to be found, the requirement of an integer number of slices per wave period leads to substantial timing constraints. In addition, the delay objects can be seen as dead time, where acquisition is not possible. Depending on the number of slices and wave-phase offsets acquired, this amounts to up to 5% of total scan duration. In order to successfully employ eXpresso, sequence parameters such as the wave frequency, number of slices, echo time, spoiling area, readout bandwidth, and encoding fraction have to be tuned such that they fit into the scheme. While an optimal set of sequence parameters can be found, the process of finding these parameters can be cumbersome and is not straightforward.

In this work, we propose a generalization of the eXpresso scheme termed *Ristretto* that enhances sequence timing flexibility by eliminating the sequence dead time through incorporating the delay into each imaging shot and additionally allowing for the interleaved acquisition of wave phases. Thereby, accelerated multi-slice MRE acquisitions become possible independent of the number of slices acquired, and sequence parameter optimization is simplified. The gain in flexibility is demonstrated for typical use cases of GRE-MRE, and the sequence is validated in a phantom study and in vivo feasibility is demonstrated.

2 | THEORY

In mono-frequency MRE, the spins are subject to periodic motion of a single frequency f. Their displacement is given by

$$\vec{r}(\vec{x}, t) = \vec{r}_0(\vec{x}) \sin\left(2\pi f t + \theta(\vec{x})\right), \tag{1}$$

where $\vec{r}_0(\vec{x})$ is the local displacement amplitude, f the frequency of the wave, and $\theta(\vec{x})$ the local wave phase. In multi-slice MRI, N_S slice excitations are interleaved to maximize the per-slice repetition time, reducing partial saturation effects and increasing the SNR. In a conventional GRE-MRE sequence, the imaging shot duration is forced to be an integer multiple of the wave period of the wave to ensure synchronization of the acquisition and actuation (see Figure 1A).[1,31] Temporal shifting of the sequence with respect to the onset of wave actuation allows to acquire the different wave-phase offsets necessary for successful wave displacement field recovery. In order to reduce total scan duration in multi-slice GRE-MRE, Garteiser et al proposed eXpresso MRE, a multi-shot sequence with fractional encoding.[30] Here instead of only one slice, an integer number of slices N_{SPP} per wave period $T = f^{-1}$ is acquired as depicted in Figure 1B.

Generally, the eXpresso sequence is built from imaging shots IS(s_d, φ_p, k_y, e) of equal duration (see Figure 1F), each acquiring a different combination of slice s_d, wave-phase offset φ_p, *k*-line k_y, and encoding direction e. The slice ordering in each multi-slice train, i.e. the subsequent acquisition of all slices $s_1 \ldots s_{N_S}$ for a fixed triplet (φ_p, k_y, e), is given by i_d, where slice s_d is acquired at the ith position in the train. The N_P equidistant wave-phase offsets $\varphi_p = 2\pi N_P^{-1} p$ ($p \in \{0 \ldots N_P - 1\}$) are acquired by introducing a delay T/N_P after each multi-slice train. Hence, the wave-phase offsets are acquired in ascending order with

$$p_{n+1} = (p_n + 1) \bmod N_P, \tag{2}$$

where n counts the successive multi-slice trains. Thus, the displacement field with respect to the start of each imaging shot IS$\left(s_d, \varphi_{p_n}, k_y, e\right)$ is given by

$$\vec{r}_{d,p_n}(\vec{x}, \tau) = \vec{r}_0(\vec{x}) \sin\left(2\pi f \tau + \theta(\vec{x}) + \underbrace{\Delta\varphi i_d}_{\text{Slice reference phase}} + \underbrace{2\pi N_P^{-1} p_n}_{\text{Wave offset } \varphi_{p_n}}\right). \tag{3}$$

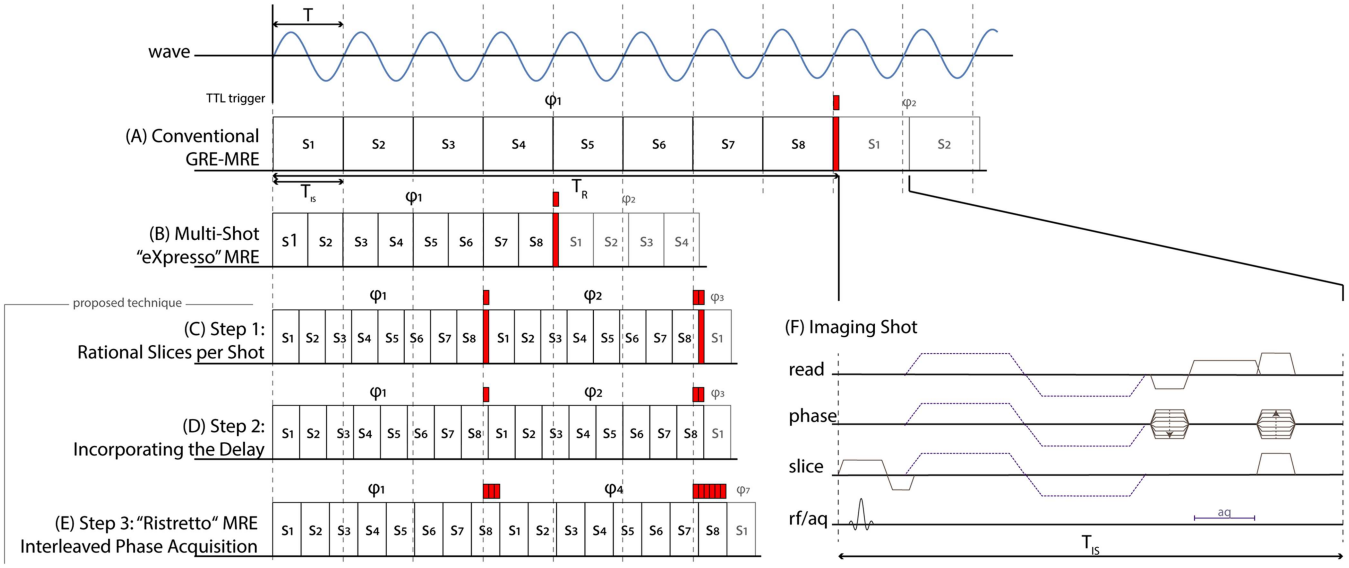

FIGURE 1 Timing diagram comparison of the proposed Ristretto multi-shot sequence (C-E), with conventional (A), and eXpresso multi-slice (B), GRE-MRE. Each square denotes a fractional GRE-MRE imaging shot (F), acquiring one *k*-line for one encoding direction, slice, and wave-phase offset. The full MRE dataset is acquired in four loops, their ordering being from innermost to outermost: Slice, wave phase, *k*-line, and encoding direction. Red squares above the diagrams denote the shift in wave phase. Red markers within the sequence diagram denote delay objects, which are introduced into the sequence to shift the multi-slice acquisition with respect to the trigger of the wave. A TTL is sent for each *k*-line and encoding direction after all wave-phase offsets and slices are acquired

Each imaging shot is of fixed duration, which is given by

$$T_{\mathrm{IS}} = \frac{T}{N_{\mathrm{SPP}}} \tag{4}$$

and the constraint that the slices per wave period N_{SPP} must be a divisor of the total number of slices N_{S}, i.e.

$$N_{\mathrm{S}} \equiv 0 \pmod{N_{\mathrm{SPP}}}. \tag{5}$$

The effective per-slice repetition time T_{R} is given by

$$T_{\mathrm{R}} = T\left(\frac{N_{\mathrm{S}}}{N_{\mathrm{SPP}}} + \frac{1}{N_{\mathrm{P}}}\right). \tag{6}$$

For successful recovery of the displacement field, the slice reference phase needs to be accounted for before wave inversion. The difference in slice reference phase between successive imaging shots is given by

$$\Delta\varphi = 2\pi\frac{T_{\mathrm{IS}}}{T} = \frac{2\pi}{N_{\mathrm{SPP}}}. \tag{7}$$

2.1 | Rational slices per wave period

Successful acquisition of an MRE dataset requires wave-phase consistency for each acquired slice, wave-phase offset, and encoding direction separately. Hence, the eXpresso concept can be first generalized by acknowledging, that the total duration of all imaging shots for the same phase offset, *k*-line, and encoding direction can be chosen as an integer multiple of the wave period. Thus, an arbitrary number of slices N_{S} can be acquired within an arbitrary number of wave periods N_{W} (Figure 1C). The number of slices per wave period N_{SPP} is then given by a rational number

$$N_{\mathrm{SPP}} = \frac{N_{\mathrm{S}}}{N_{\mathrm{W}}}. \tag{8}$$

Here, imaging shot duration T_{IS}, per-slice repetition time T_{R}, and phase-offset $\Delta\varphi$ are equivalently defined as in the eXpresso scheme.

2.2 | Incorporating the delay into the imaging shot

The delay object, which shifts the sequence with respect to the external wave to acquire the wave-phase offsets, can be omitted by distributing its duration evenly over all imaging shots of one multi-slice train (Figure 1D). Thereby, the imaging shot duration is slightly increased, while the per-slice repetition time is kept constant. The imaging shot duration is then given by

$$T_{\mathrm{IS}} = T\left(\frac{N_{\mathrm{W}}}{N_{\mathrm{S}}} + \frac{1}{N_{\mathrm{P}}N_{\mathrm{S}}}\right). \tag{9}$$

The per-slice repetition time is unchanged, but is now best expressed in terms of the number of wave periods N_W:

$$T_R = T\left(N_W + \frac{1}{N_P}\right). \tag{10}$$

The phase offset between successively acquired slices is given by

$$\Delta\varphi = 2\pi\left(\frac{N_W}{N_S} + \frac{1}{N_P N_S}\right). \tag{11}$$

2.3 | Interleaved phase acquisition: Ristretto MRE

The incorporation of the delay into the imaging shot duration allows sequence timing flexibility to be increased by interleaved acquisition of the wave-phase offsets φ_{p_n}. To this end, the sequence delay is extended by an integer factor $N_D < N_P$ (Figure 1E). The recurrence equation (Equation 2) for the wave-phase offsets is then replaced by

$$p_{n+1} = (p_n + N_D) \bmod N_P. \tag{12}$$

Since no further delay objects are introduced and all imaging shots are of the same duration, it must be assured that all phase offsets are acquired. This is fulfilled only by delays N_D that are co-primes of N_P, i.e.

$$N_D,\ N_P \text{ are co-prime} \Leftrightarrow \mathrm{GCD}(N_D, N_P) = 1 \Leftrightarrow \mathrm{LCM}(N_D, N_P) = N_D N_P, \tag{13}$$

where $\mathrm{GCD}(\cdot,\cdot)$ denotes the greatest common divisor and $\mathrm{LCM}(\cdot,\cdot)$ the least common multiple. Proof is given in the appendix.
Elongating the delay increases the timing flexibility of the imaging shot to

$$T_{IS} = T\left(\frac{N_W}{N_S} + \frac{N_D}{N_P N_S}\right) \tag{14}$$

and the per-slice-repetition time becomes

$$T_R = T_{IS} N_S = T\left(N_W + \frac{N_D}{N_P}\right). \tag{15}$$

The wave phase-offset is determined by Equation 7 and evaluates to

$$\Delta\varphi = 2\pi\left(\frac{N_W}{N_S} + \frac{N_D}{N_P N_S}\right). \tag{16}$$

3 | METHODS

The proposed Ristretto sequence was implemented on a Philips 3 T systems (Philips Healthcare, Best, The Netherlands). Experimental data were acquired in a gel phantom (CIRS, Norfolk, VA, USA) using the proposed Ristretto scheme, as well as conventional GRE-MRE and where applicable the eXpresso sequence.[30] In vivo data were collected in the breast and liver in one healthy volunteer upon informed consent and according to institutional guidelines using both the Ristretto and eXpresso schemes. Fractional encoding[29] with bipolar motion encoding gradients (MEGs) was used for motion sensitization and the external actuator was phase-locked to the sequence using a transistor-transistor logic (TTL) trigger.

The phantom scans were performed using electro-magnetic actuation (25, 36, 40, and 60 Hz), eight wave-phase offsets, 180 Hz bipolar MEGs, 16.6 mT/m MEG strength, motion encoding of 7.06 rad/mm, and four encoding directions following the Hadamard encoding scheme.[28] The signal was received using a 15-channel head coil. Imaging parameters were 13 to 17 slices, 3 mm isotropic resolution, a 64 × 52 acquisition matrix acquired with Cartesian readout and 2× SENSE parallel imaging acceleration[32] resulting in a field of view (FOV) of 192 × 156 × 39–51 mm^3, and a flip angle of 20°, as well as RF-spoiling. In order to maximize SNR and to eliminate water/fat-dependent signal phase offsets, the echo time was chosen as the third in-phase condition of water/fat, i.e. 6.91 ms on a 3 T Philips system.

Three different phantom studies were performed. First, five scans were performed acquiring 14 slices to compare conventional GRE-MRE, eXpresso MRE, and the proposed sequence generalizations illustrated in Figure 1. The sequence timing parameters for the five scans are given as part of the results in Figure 4 later. Total acquisition time was reduced from 5 min 28 s for conventional MRE to 2 min 46 s for eXpresso MRE and 1 min 59 s for generalization steps 1 and 2. Ristretto MRE acquired the same displacement field in 1 min 42 s, equivalent to a 3.2-fold acceleration compared with conventional GRE-MRE.

The second phantom study compares the performance of conventional, eXpresso, and Ristretto MRE with regards to different wave frequencies. Here, 15 slices were acquired with 25, 36, 40, and 60 Hz wave frequencies, while all other imaging parameters were held constant. Sequence timing parameters for the Ristretto acquisition were N_W/N_D = 3/3 (25 Hz), 4/7 (36 Hz), 5/3 (40 Hz), and 7/7 (60 Hz). Note that eXpresso can only be employed under the conditions chosen for the sequence comparison at 25 and 36 Hz wave frequencies, and was performed with N_{SPP} = 3.

The third phantom study compares the performance of the three sequence types with regards to different numbers of acquired slices. Here, the wave frequency and all other imaging parameters were held constant, while the number of slices was changed consecutively from 13 to 17. Sequence timing parameters for the Ristretto acquisition were N_W/N_D = 4/1 (13 slices), 4/3 (14 slices), 4/7 (15 slices), 5/1 (16 slices), and 5/3 (17 slices). Under these conditions, eXpresso with two shots per period can only be employed with 14 and 16 acquired slices, while three shots per period can be achieved for 15 slices.

The breast scan was performed with 36 Hz gravitational actuation,[33] eight wave-phase offsets, 180 Hz MEG frequency, 19.7 mT/m MEG strength, motion encoding of 8.2 rad/mm, and unbalanced four-point encoding. Signal was received using a seven-channel breast coil. Imaging parameters were 15 slices, 2 mm isotropic resolution, a 176 × 69 acquisition matrix acquired with 2× SENSE acceleration[32] resulting in an FOV of 352 × 138 × 30 mm^3, Cartesian readout, and a flip angle of 20°. The echo time was chosen as the third in-phase condition of water/fat at 3 T, i.e. 6.91 ms. The breast acquisition was performed with an optimized eXpresso scheme (N_{SPP} = 3) and compared with Ristretto with N_W = 4 and reverse phase ordering (N_D = 7, N_{SPP} = 3.08), leading to a total scan duration of 6 min 28 s for eXpresso and 6 min 9 s for Ristretto.

The liver scan was performed with 50 Hz gravitational actuation,[33] four wave-phase offsets, 260 Hz MEG frequency, 18.9 mT/m MEG strength, motion encoding of 5.15 rad/mm, and Hadamard encoding.[28] Signal was received using a 32-channel cardiac coil. Imaging parameters were nine slices, 4 mm isotropic resolution, an 80 × 54 acquisition matrix acquired with 1.48× SENSE acceleration,[32] Cartesian readout, and a flip angle of 20°, resulting in an FOV of 320 × 216 × 36 mm^3. The echo time was chosen as the second in-phase condition of water/fat on a Philips 3 T system, i.e. 4.60 ms. The liver acquisition was performed with an optimized eXpresso scheme (N_{SPP} = 3) and compared with Ristretto with N_W = 2 and reverse phase ordering (N_D = 3, N_{SPP} = 3.27). The full displacement field was acquired for each scan within four breath holds (BHs) of 14.5 s for eXpresso and 12.3 s for Ristretto. After reconstruction, displacement fields were obtained through temporal unwrapping of the signal phase, decoding, and subsequent temporal Fourier transformation. The displacements were phase corrected according to the eXpresso and Ristretto slice reference phases. For both in vivo scans, shear wave velocities were obtained using a FEM-based inversion algorithm after smoothing of the displacement fields using an isotropic Gaussian filter of width σ = 0.5 pixel (breast) and σ = 0.75 pixel (liver).[34]

4 | RESULTS

In Figure 2, conventional eXpresso and Ristretto multi-slice GRE-MRE schemes are compared with regard to achievable imaging shot duration for the typical case of eight wave-phase offsets and different slice numbers (8, 10, 12, and 15). Assuming in-phase water/fat echo-time conditions on a 3 T Philips system and including an overhead time of 1.4 ms for RF pulse, readout, and spoiling leads to four different cut-off values for the

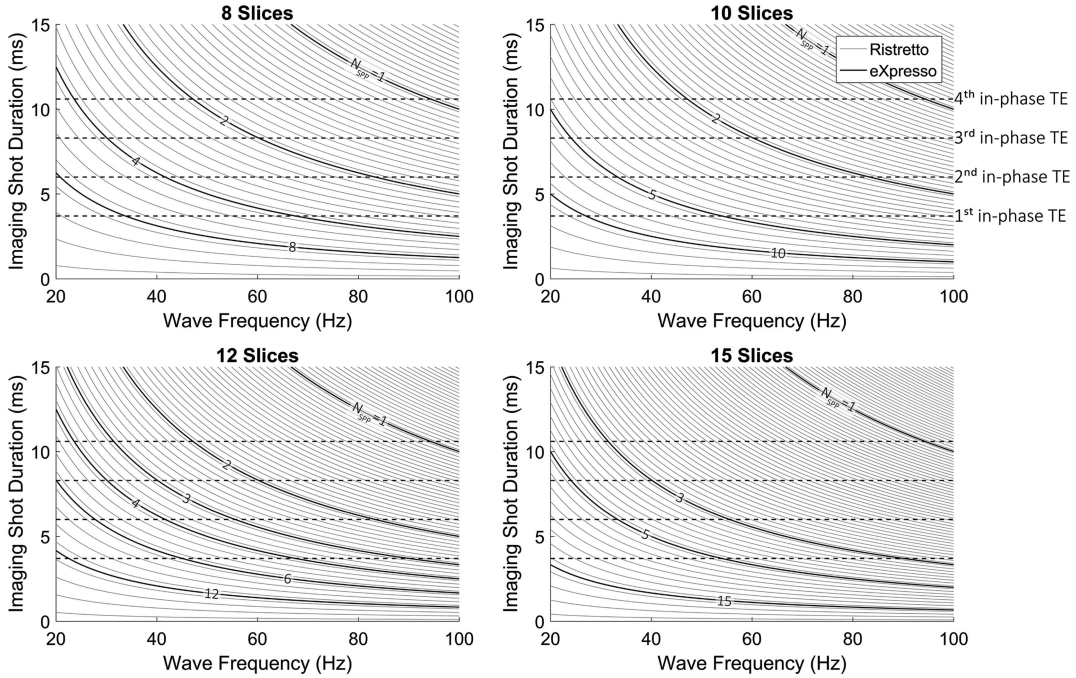

FIGURE 2 Possible imaging shot durations as a function of wave frequency for conventional MRE (thick black, N_{SPP} = 1), eXpresso MRE (thick black) and Ristretto MRE (gray) for 8, 12, 10, and 15 slices and assuming eight wave-phase offsets. The topmost black line corresponds to the conventional MRE case, where one slice is acquired per wave period. Depending on the wave frequency and number of slices, eXpresso only allows for very large steps in imaging shot duration or cannot be applied at all for frequencies above 60 Hz, whereas Ristretto allows for the fine-tuning of imaging shot durations at all frequencies. In addition, eXpresso does not allow for the acquisition of less than one slice per wave cycle, limiting applicability of MRE at high frequencies (>100 Hz). The black dashed lines denote cut-off values for the first four water/fat in-phase echo times at 3 T and additional overhead time of 1.4 ms for RF pulse, readout, and spoiling. The graphs can be used as a look-up table to find an optimal wave frequency for a given set of imaging parameters

imaging shot duration (3.7, 6, 8.3, and 10.6 ms), which are overlaid as broken lines. The water/fat in-phase condition was chosen to maximize SNR and to eliminate water/fat-dependent signal phase offsets.[30] While eXpresso (thick black lines, $N_{SPP} > 1$) only allows for a very limited number of imaging shot durations, the imaging shot duration in Ristretto can be chosen on a fine grid (gray lines). In the case of 15 slices, this amounts to 40 subdivisions between conventional GRE-MRE ($N_{SPP} = 1$) and three slices per wave period (second black line). While the eXpresso scheme generally fails above approximately 60 Hz assuming that the third in-phase T_E (6.9 ms) is chosen to allow for sufficient motion encoding, Ristretto can reduce total acquisition duration even at 100 Hz.

In Figure 3, imaging shot duration (A) and the duration for the acquisition of all slices and phases per *k*-line and encoding direction (B) are shown as a function of the number of slices for three wave frequencies (36, 60, and 100 Hz) and four imaging shot durations corresponding to the four aforementioned in-phase cut-off times. Depending on the number of slices, typically one or two accelerated options exist in the eXpresso scheme (crosses). If the number of slices is a prime number, application of the eXpresso scheme is not possible. In contrast, due to the increased timing flexibility of the Ristretto scheme (dots), acceleration is possible independent of the number of slices acquired, and the scheme allows for a large range of imaging shot durations. In addition, Ristretto allows for the elongation of the imaging shot duration beyond the one wave-period limit, which permits its use at frequencies where the wave period becomes shorter than the imaging shot duration (here >120 Hz for the third in-phase condition). In Supporting Figure S1, Figure 3A is presented for different numbers of wave-phase offsets (3 to 8).

4.1 | Phantom validation

In Figure 4, the real part of the complex displacement field measured in the phantom is compared for the five sequences presented in Figure 1 and presented together with the sequence timing parameters, total scan duration, and corresponding acceleration factor compared with conventional MRE. In Figure 4-1, the in-plane displacement is shown after correcting for the acquisition phase offset $\Delta\varphi$. With the chosen echo time of 6.91 ms, 36 Hz wave frequency, and 14 acquired slices, conventional GRE-MRE requires 5 min 28 s to acquire the full 3D displacement field. eXpresso MRE permits the acquisition to be accelerated with two imaging shots per wave period, leading to a 1.98-fold acceleration. Acquisition of a rational number of slices per wave period (Step 1, Figure 1C) allows 14 slices to be acquired in five instead of seven wave periods. Incorporating the delay object into the sequence (Step 2, Figure 1D) does not change the overall acquisition duration of the sequence. Both lead to 2.76× faster acquisition than conventional MRE. With interleaved acquisition (Step 3, Figure 1E) the 14 slices are acquired in four wave periods, and the wave phases are acquired in interleaved ordering ($N_D = 3$), leading to 3.22-fold acceleration compared with conventional GRE-MRE (1 min 42 s). The wave fields of all four acquisition techniques are in excellent agreement.

In Figure 4-2, a through-plane view of the displacement fields is shown *before* the application of the phase correction. The displacement fields are inconsistent, as each slice is acquired with a different reference time-point within the wave cycle (Equation 3). Figure 4-3 shows the same displacement field *after* correcting for the slice reference phase offset $\Delta\varphi i_d$, again showing excellent agreement between the techniques.

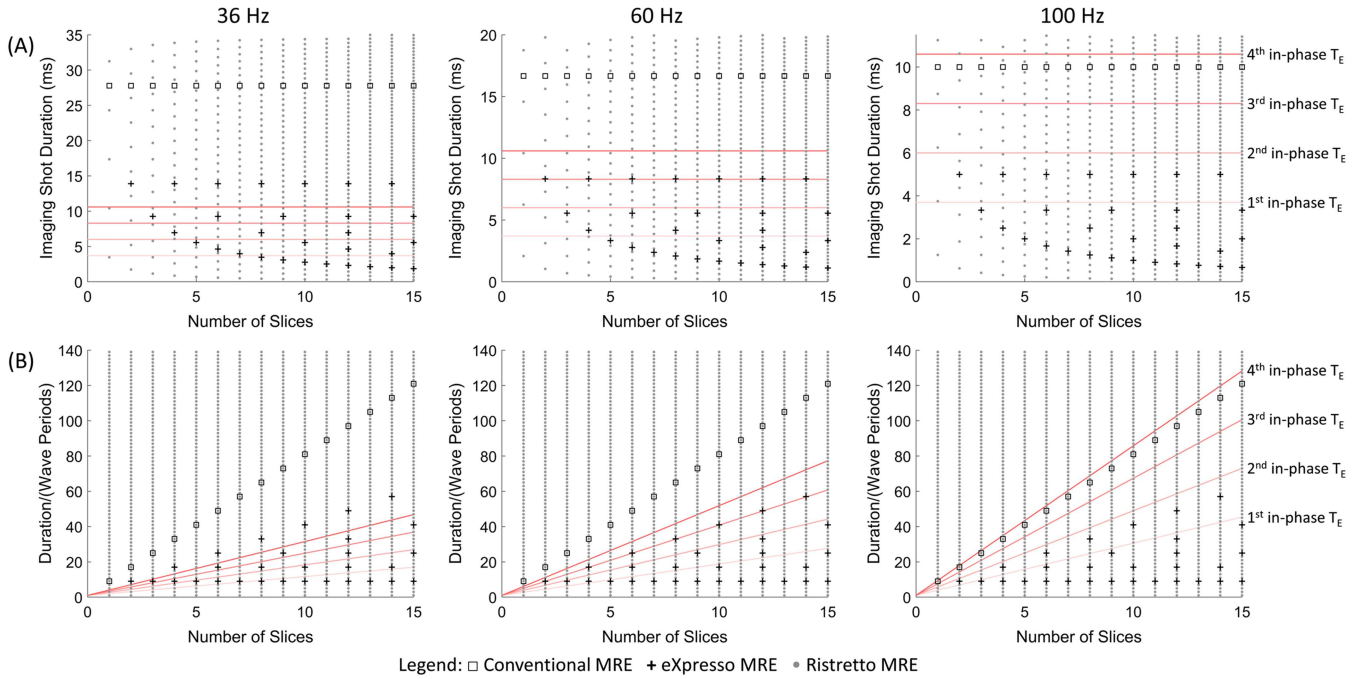

FIGURE 3 Sequence timing options for eight wave-phase offsets acquired with conventional MRE (black square), eXpresso MRE (black cross) and Ristretto MRE (gray dot) for 36, 60, and 100 Hz. Imaging shot duration (A), and acquisition duration in units of the wave period (B), versus the number of acquired slices. Cut-off values for the imaging shot duration are plotted for the first four water/fat in-phase conditions including a 1.4 ms overhead for the RF pulse, readout, and spoiling, providing a lower limit for the imaging shot duration. The graphs can be used as a look-up table for finding optimal imaging parameters for a given wave frequency

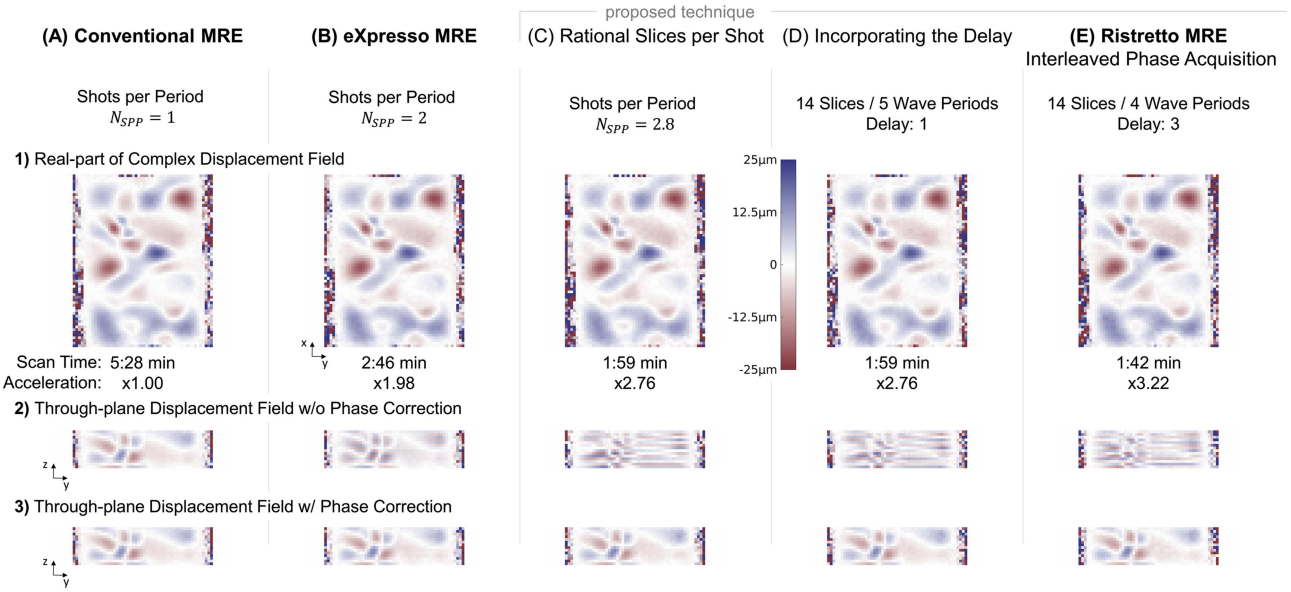

FIGURE 4 1), comparison of the real parts of the complex displacement field, scan time, and acceleration of conventional GRE-MRE (A), eXpresso MRE (B), and the three generalization steps to Ristretto MRE after phase correction (C-E). In all cases 14 slices were acquired at 36 Hz wave frequency and using equal imaging parameters. Displacement fields are in excellent agreement for all six MRE sequences. 2), through-plane view of the same acquisitions without per-slice phase correction showing the effect of the accelerated acquisition on the acquired wave phase; 3), respective through-plane displacement fields after phase correction

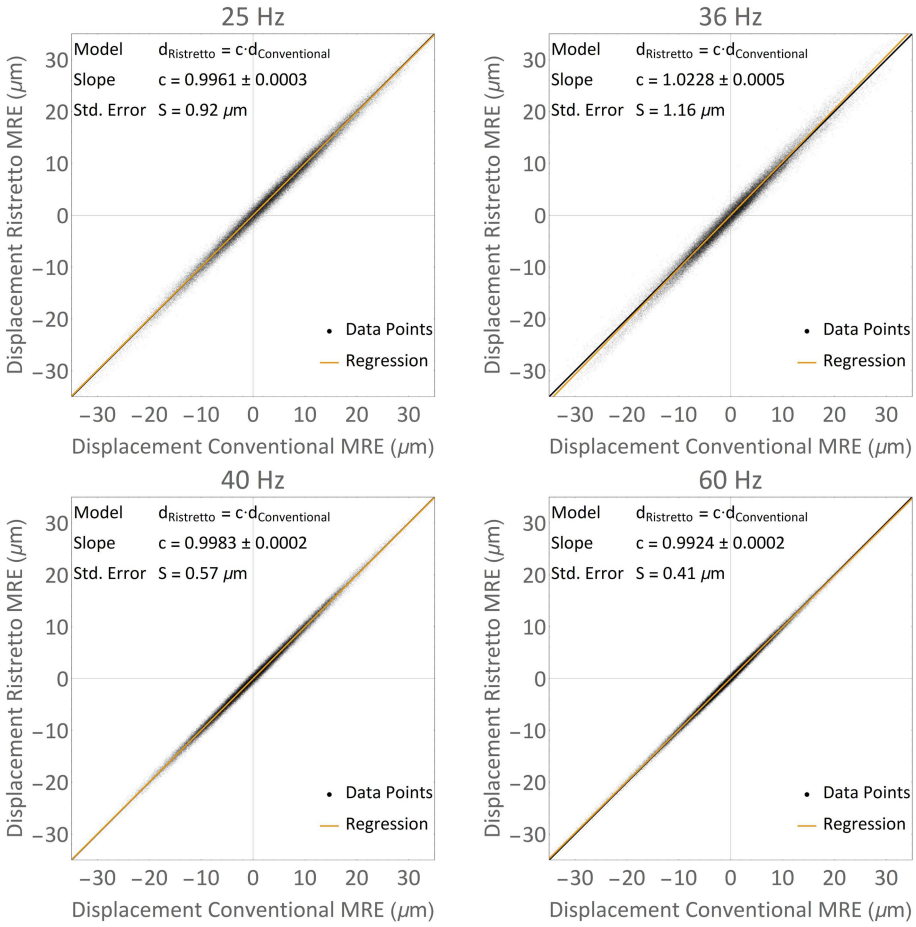

FIGURE 5 Correlation of the real parts of the complex displacement vector measured with conventional and Ristretto MRE for 25, 36, 40, and 60 Hz wave frequencies, showing excellent agreement of the two techniques. The diagonal of the correlation plot is shown in black, closely coinciding with the regression analysis. Sequence timing parameters for the Ristretto acquisition were the following: 25 Hz, N_W/N_D = 3/3 (1 min 53 s); 36 Hz, N_W/N_D = 4/7 (1 min 53 s); 40 Hz, N_W/N_D = 5/3 (1 min 53 s); 60 Hz, N_W/N_D = 7/7 (1 min 50 s). The scan durations for the conventional MRE scans were the following: 25 Hz, 8 min 26 s; 36 Hz, 5 min 52 s; 40 Hz, 5 min 17 s; 60 Hz, 2 min 31 s

In Figure 5, correlation plots of the real parts of the complex displacement field vector measured with conventional and Ristretto MRE are shown for 25, 36, 40, and 60 Hz wave frequencies. A linear regression analysis was performed to determine the correlation coefficient, its standard deviation, and the standard error of the fit. Results are given alongside the correlation plots. Correlation coefficients are very close to one, ranging from 0.9924 to 1.0228. The standard error of the fit for 40 and 60 Hz was lower than 0.6 μm, which is less than 2% of the peak displacement amplitude of 30 μm. For 25 and 36 Hz, the standard error of the fit was slightly elevated, measuring 0.92 and 1.16 μm. The relative standard errors of the fit are within the same domain as in a previously published correlation study utilizing GRE-MRE.[28]

In Figure 6, the scan durations for the slice (A) and frequency (B) studies are compared between the three acquisition techniques. In the slice study, Ristretto allows for approximately 3.2-fold acceleration of the MRE scan independent of the number of slices. Additionally, conventional and Ristretto MRE show an approximately linear scan time increase with increasing number of slices. eXpresso MRE on the other hand, can only be used for 14, 15, and 16 slices, with minimal scan duration for 15 slices. Total scan duration in the conventional MRE case drops inversely with the wave frequency, while the duration of the respective Ristretto acquisition remains approximately constant. Since 15 slices are acquired, eXpresso can accelerate the scan by approximately threefold; however, it fails above 36 Hz as the wave period becomes less than three times the minimal repetition time. The root-mean-square error (RMSE) of the real part of the complex displacement field is also shown for eXpresso and Ristretto, where the conventional MRE scan serves as ground truth. For all scans, the RMSE is below 5% of the peak amplitude (30 μm) and is comparable between all techniques. In all cases, Ristretto MRE outperforms eXpresso MRE in terms of scan duration.

4.2 | In vivo validation

In Figure 7, the eXpresso and Ristretto acquisition schemes are demonstrated in the in vivo breast. Since the MRE protocol was optimized for the use of eXpresso MRE, effective per-slice repetition times are nearly equivalent for eXpresso with three slices per wave period and Ristretto with $N_W = 4$ and $N_D = 7$. Contrast and SNR are equivalent in the two acquisitions and total speed-up amounts to only 5% in this case. The real parts of the complex displacement field and the recovered shear wave velocities are in good agreement, resulting in ROI-averaged velocities of 0.46 ± 0.29 m/s for eXpresso and 0.45 ± 0.28 m/s for Ristretto MRE. The rightmost column of Figure 7 shows the through-plane displacement fields for both scans before and after correction of the acquisition phase offset $\Delta\varphi$ for one representive position in the breast, demonstrating successful recovery of the displacement fields.

In Figure 8, a comparison of eXpresso and Ristretto MRE is given for the in vivo liver. Again, the protocol was first optimized for the use of eXpresso, leading to a BH duration of 14.5 s. Switching to Ristretto MRE, the BH duration could be reduced to 12.3 s, which is equivalent to a 15% reduction in scan duration. Both the real parts of the displacement fields and the shear velocity maps and ROI-averaged values (eXpresso, 1.39 ± 0.09 m/s; Ristretto, 1.37 ± 0.09 m/s) are in good agreement. An additional through-plane view of the real parts of the displacement fields before and after phase correction is shown in the rightmost column of Figure 8. Again, good agreement between the two techniques could be found.

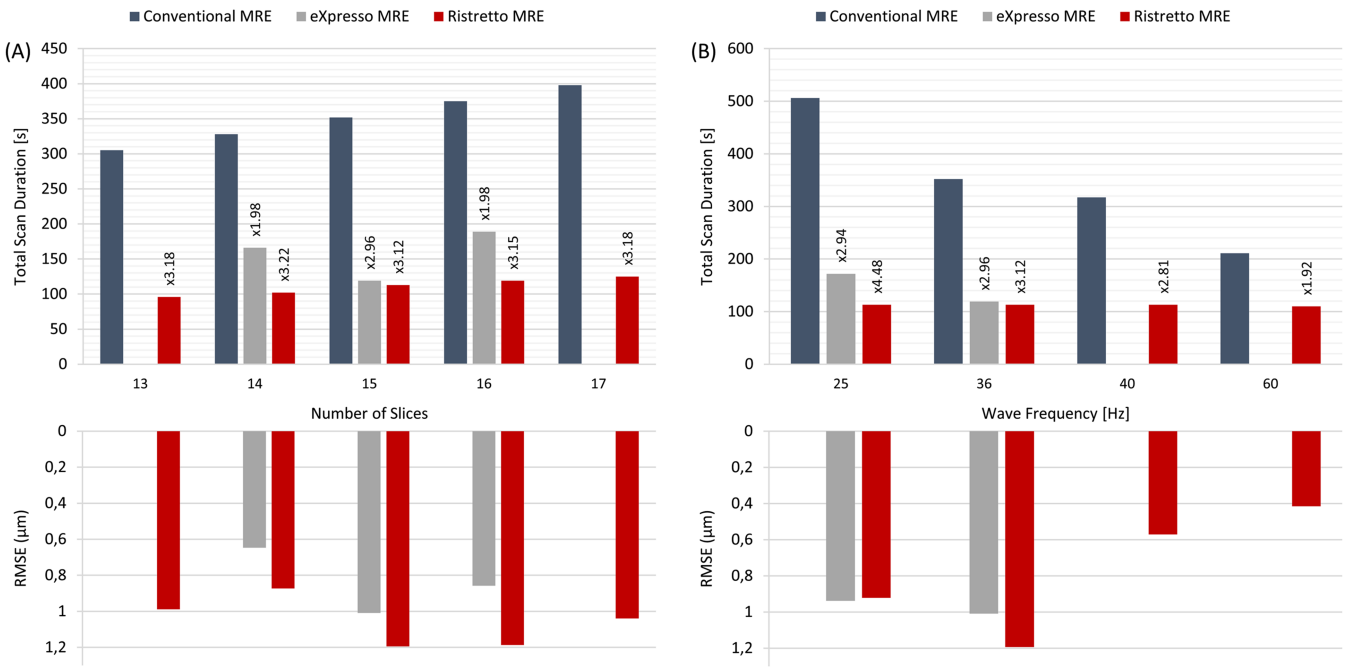

FIGURE 6 Comparison of phantom scan durations and RMSEs of the real part of the complex displacement field for different numbers of acquired slices (A), and change in wave frequency (B). The slice study was conducted at 36 Hz, while the frequency study was conducted measuring 15 slices, while all other imaging parameters were held constant. The data labels above the eXpresso and Ristretto bars denote accelerations compared with the respective conventional MRE acquisition. For 13 and 17 slices, as well as 40 and 60 Hz, eXpresso MRE cannot be used. Ristretto MRE (red) can substantially accelerate acquisition in all cases (1.92- to 4.48-fold acceleration compared with conventional MRE) and always shows lower acquisition time than eXpresso MRE. For all scans, RMSE is below 5% of the peak amplitude (30 μm)

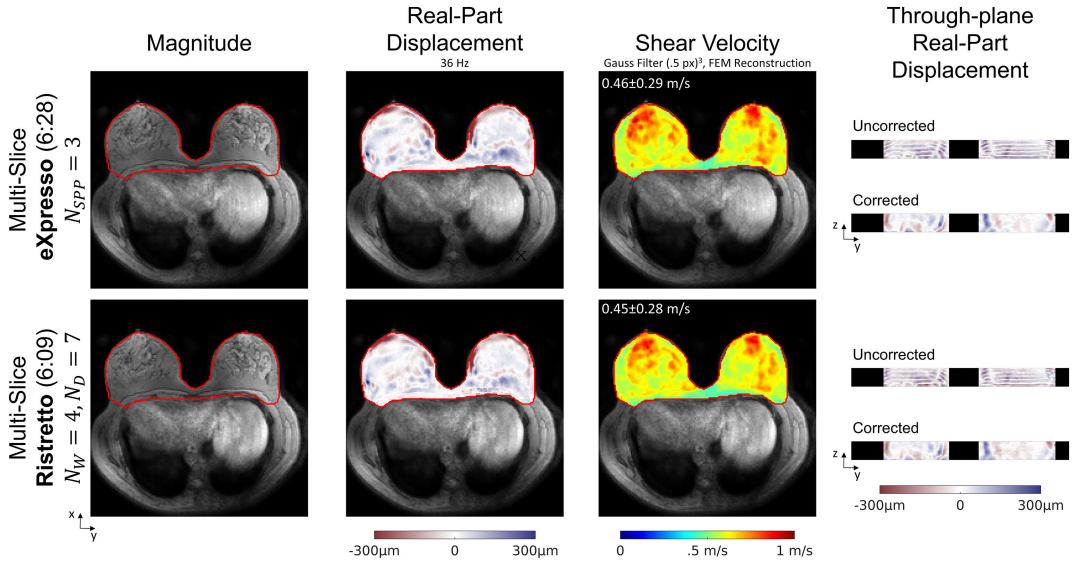

FIGURE 7 Comparison of eXpresso and Ristretto multi-slice MRE in vivo. Magnitude images have equal contrast and SNR due to the same flip angle and approximately equal per-slice repetition time of the two scans. The real part of the complex displacement field is shown for the same slice as the magnitude image on the left, while shear wave velocity was averaged over the innermost nine slices. Both the real parts of the displacement field and the shear velocities are in good agreement. The rightmost column shows through-plane views of the displacement fields before and after phase correction for visualization of the phase-correction procedure. After correction, displacement fields are again in good agreement between the two techniques

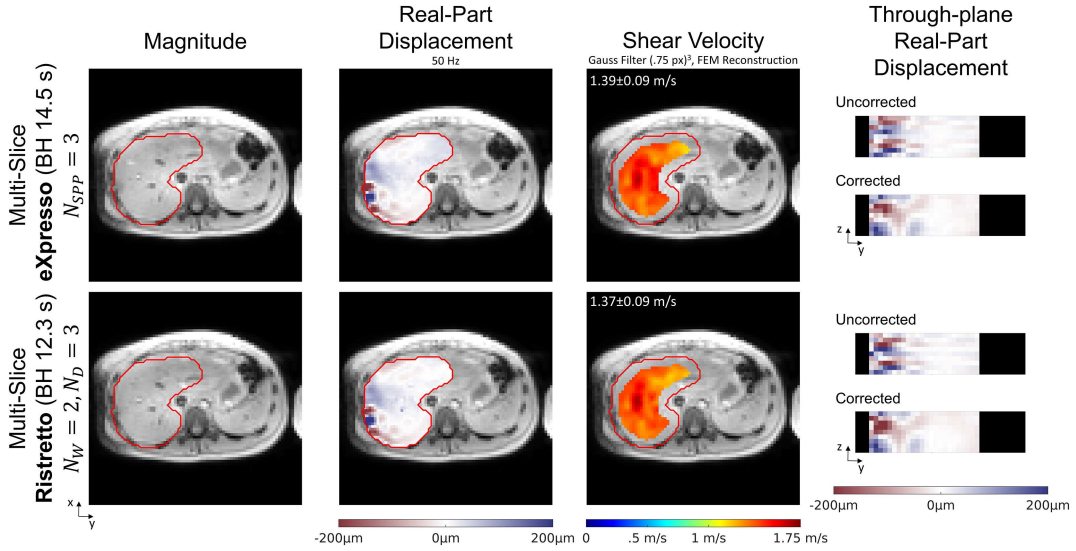

FIGURE 8 Comparison of eXpresso and Ristretto multi-slice MRE in the liver. Magnitude images have equal contrast and SNR due to the same flip angle and approximately equal per-slice repetition time of the two scans. The real part of the complex displacement field is shown for the same slice as the magnitude image on the left, while shear wave velocity was averaged over the innermost five slices. Both the real parts of the displacement field and the shear velocities are in good agreement. The rightmost column shows through-plane views of the displacement fields before and after phase-correction for visualization of the phase correction procedure. After correction, displacement fields are again in good agreement between the two techniques

5 | DISCUSSION

In this work it has been demonstrated that Ristretto MRE allows for the fine-tuning of imaging shot duration and hence acquisition time in conventional MRE. Since the eXpresso timing can be reproduced using the Ristretto approach, the eXpresso scheme can never outperform Ristretto. While efficient eXpresso accelerations can be found for most frequencies below about 60 Hz, the process of finding a suitable combination of number of slices, slices per wave period, MEG duration, echo time, readout bandwidth, and total acquisition time can be cumbersome. With the use of Ristretto, the imaging shot duration can be independently minimized for every sequence parameter combination, retaining most of the imaging flexibility known from conventional MRI.

We demonstrated in phantom experiments as well as in in vivo scans that the change in sequence timing and wave-phase ordering does not substantially influence overall MRE data quality and leads to good agreement in both displacement fields and recovered shear velocities. For the

in vivo comparison, the eXpresso scheme was first optimized to make best use of its reduced timing flexibility. Starting from there, Ristretto was used to further reduce acquisition duration. Hence, overall scan time reduction in the breast scan was limited to only 5%. The phantom study was also acquired with optimal conditions for the eXpresso sequence (number of slices dividable by three and 36 Hz wave frequency). However, the slice study shows that changes to the FOV can lead to significant scan time increases when eXpresso MRE is used. Equivalently, increasing the FOV in the eXpresso MRE breast scan to 16 and 17 slices leads to an increase in scan duration of approximately 160% (2 shots per period) and 340% (conventional MRE) compared with the 15 slice eXpresso case. Optimal conditions are only found again for 18 slices, increasing scan duration by 120% (three shots per period). With the use of Ristretto, scan time increases approximately proportionally to the number of slices acquired, which amounts to 97% (16 slices), 102% (17 slices), and 112% (18 slices) compared with the 15 slice eXpresso case. Hence, Ristretto allows an optimal MRE protocol to be found matching the exact FOV requirements for any given case.

Ristretto permits the imaging shot duration to be increased beyond the one wave period limit. This allows GRE-MRE for high frequency MRE acquisitions, where slice excitation, motion sensitization, readout, and spoiling combined exceed the wave period. Thus, in contrast to eXpresso, Ristretto enables pre-clinical GRE-MRE studies on full-body systems with limited slew and gradient strength capabilities that necessitate the use of multiple MEG repetitions.

In addition, the increased timing flexibility of Ristretto MRE allows elastograms to be acquired at any given wave frequency with approximately equal repetition times and otherwise identical imaging parameters. Hence, image contrast, SNR, off-resonance artifacts, eddy-current-induced phase errors, and distortions are equal. This might prove vital in sequential multi-frequency MRE, where geometric consistency is key to successful wave inversion.[35,36]

The original work by Garteiser et al demonstrated eXpresso MRE also for multi-frequency MRE, where the wave field also contains higher harmonics *mf* while the different wave-field components are separated using the Fourier transformation.[30] For each harmonic, Equation 3 holds separately with $f \rightarrow mf$,

$$\vec{r}_{d,p_n,\boldsymbol{mf}}\left(\vec{x},\tau\right) = \vec{r}_0\left(\vec{x}\right)\sin\left(2\pi\boldsymbol{mf}\tau + \theta\left(\vec{x}\right) + \Delta\varphi i_d + 2\pi N_p^{-1}p_n\right). \tag{17}$$

Hence, the Ristretto scheme can equally be applied to multi-frequency MRE, where each frequency component has to be corrected with the same slice reference time offset $\Delta\varphi$.

The interleaved acquisition of wave-phase offsets is key to increasing sequence timing flexibility. If the number of phases is a power of two, any uneven number can be chosen, which allows for imaging shot adjustments of

$$\Delta T_\mathrm{R} = \frac{2T}{N_\mathrm{P}N_\mathrm{S}} \quad \text{with} \quad N_\mathrm{P} = 2^n,\ n \in \mathbb{N} \tag{18}$$

In a typical 10 slice, eight phase-offset acquisition, this amounts to

$$\Delta T_\mathrm{R}^{N_\mathrm{S}=10,N_\mathrm{P}=8} = \frac{T}{40}.$$

Given that the number of acquired wave phases is a prime number, e.g. 3, 5, 7, or 11, the delay can be any number smaller than N_P, allowing for maximal timing flexibility of

$$\Delta T_\mathrm{R} = \frac{T}{N_\mathrm{P}N_\mathrm{S}} \quad \text{with} \quad N_\mathrm{P} \in \text{primes}. \tag{19}$$

The acquisition of six wave-phase offsets is the least flexible, as only two possibilities for the interleaved acquisition exist, i.e. the conventional non-interleaved acquisition $N_\mathrm{D} = 1$ and reversed acquisition with $N_\mathrm{D} = 5$. A graphical representation of the imaging shot duration for the different cases is presented in the supplementary material (Supplementary Figure S1).

Choosing $N_\mathrm{D} = 1$ and $N_\mathrm{W} = N_\mathrm{S}/N_\mathrm{SPP}$ in the Ristretto scheme, the eXpresso sequence is recovered. Here, the effective per-slice repetition times T_R, the wave-phase acquisition orders, and hence total acquisition durations are equivalent. Thus, the Ristretto scheme is always either equally fast or faster than eXpresso.

Choosing $N_\mathrm{S} = 1$ in the Ristretto scheme allows the concept to be applied to 3D acquisitions, where a slab is excited and phase encoding is employed along the slice direction. Here, sequence flexibility is achieved solely through the interleaved acquisition of the motion phases for the same k_y/k_z-lines. The shot duration is given by

$$T_\mathrm{R} = T_\mathrm{IS} = T\left(N_\mathrm{W} + \frac{N_\mathrm{D}}{N_\mathrm{P}}\right), \tag{20}$$

while the same rule applies for N_D as with multi-slice Ristretto. A phase correction is not necessary as all *k*-lines are acquired with the same phase offset, ensuring data consistency.

In the eXpresso scheme, different eddy current contributions can be accumulated per slice, as the sequence delay disturbs the otherwise equidistant slice acquisition. Here, the Ristretto scheme overcomes this issue by including the sequence offset in the imaging shot duration. Hence, an eddy current steady state can be established that is independent of the slice ordering and the time-point at which the slice is acquired. Since encoding

directions are sequentially acquired, eddy currents and mechanical vibrations arising from the different MEG directions can potentially bias the encoding. Future work should thus encompass further adaptation of the Ristretto sequence to allow for additional interleaved encoding directions.

The present work has demonstrated the feasibility of Ristretto MRE in the liver and breast in healthy volunteers. Future work will be directed toward assessing the performance of liver Ristretto MRE in patients, where the reduction in BH duration is expected to improve overall data quality, as well as investigating the use of the Ristretto scheme for brain, renal, prostate, or cardiac MRE.

6 | CONCLUSION

We have demonstrated that the multi-shot eXpresso concept can be generalized to allow for flexible tuning of imaging shot durations. In typical applications, the resulting Ristretto MRE scheme permits reduction of total scan durations by up to 450% relative to conventional MRE depending on the number of slices and wave frequency.

ACKNOWLEDGEMENTS

This project has received funding from the European Union's Horizon 2020 research and innovation program under Grant Agreement 668039.

The authors would like to express their gratitude towards Jurgen H. Runge at King's College London in helping with the acquisition of the MRE data.

FUNDING INFORMATION

European Union's Horizon 2020 research and innovation programme under Grant Agreement 668039.

ORCID

Christian Guenthner https://orcid.org/0000-0001-8707-7016
Marian Troelstra https://orcid.org/0000-0001-6748-4810
Ralph Sinkus https://orcid.org/0000-0002-6093-1654
Sebastian Kozerke http://orcid.org/0000-0003-3725-8884

REFERENCES

1. Muthupillai R, Lomas D, Rossman P, Greenleaf J, Manduca A, Ehman R. Magnetic resonance elastography by direct visualization of propagating acoustic strain waves. *Science*. 1995;269(5232):1854-1857. https://doi.org/10.1126/science.7569924
2. Low G. General review of magnetic resonance elastography. *World J Radiol*. 2016;8(1):59. https://doi.org/10.4329/wjr.v8.i1.59
3. Yin M, Talwalkar JA, Glaser KJ, et al. Assessment of hepatic fibrosis with magnetic resonance elastography. *Clin Gastroenterol Hepatol*. 2007;5(10):1207-1213.e2. https://doi.org/10.1016/j.cgh.2007.06.012
4. Rouvière O, Yin M, Dresner MA, et al. MR elastography of the liver: preliminary results. *Radiology*. 2006;240(2):440-448. https://doi.org/10.1148/radiol.2402050606
5. Huwart L, Peeters F, Sinkus R, et al. Liver fibrosis: non-invasive assessment with MR elastography. *NMR Biomed*. 2006;19(2):173-179. https://doi.org/10.1002/nbm.1030
6. Huwart L, Sempoux C, Salameh N, et al. Liver fibrosis: noninvasive assessment with MR elastography versus aspartate aminotransferase–to-platelet ratio index. *Radiology*. 2007;245(2):458-466. https://doi.org/10.1148/radiol.2452061673
7. Huwart L, Salameh N, ter Beek L, et al. MR elastography of liver fibrosis: preliminary results comparing spin-echo and echo-planar imaging. *Eur Radiol*. 2008;18(11):2535-2541. https://doi.org/10.1007/s00330-008-1051-5
8. Singh S, Venkatesh SK, Wang Z, et al. Diagnostic performance of magnetic resonance elastography in staging liver fibrosis: a systematic review and meta-analysis of individual participant data. *Clin Gastroenterol Hepatol*. 2015;13(3):440-451.e6. https://doi.org/10.1016/j.cgh.2014.09.046
9. Singh S, Venkatesh SK, Loomba R, et al. Magnetic resonance elastography for staging liver fibrosis in non-alcoholic fatty liver disease: a diagnostic accuracy systematic review and individual participant data pooled analysis. *Eur Radiol*. 2016;26(5):1431-1440. https://doi.org/10.1007/s00330-015-3949-z
10. Talwalkar JA. Elastography for detecting hepatic fibrosis: options and considerations. *Gastroenterology*. 2008;135(1):299-302. https://doi.org/10.1053/j.gastro.2008.05.038
11. Talwalkar JA, Yin M, Fidler JL, Sanderson SO, Kamath PS, Ehman RL. Magnetic resonance imaging of hepatic fibrosis: emerging clinical applications. *Hepatology*. 2008;47(1):332-342. https://doi.org/10.1002/hep.21972
12. McKnight AL, Kugel JL, Rossman PJ, Manduca A, Hartmann LC, Ehman RL. MR elastography of breast cancer: preliminary results. *Am J Roentgenol*. 2002;178(6):1411-1417. https://doi.org/10.2214/ajr.178.6.1781411
13. Xydeas T, Siegmann K, Sinkus R, Krainick-Strobel U, Miller S, Claussen CD. Magnetic resonance elastography of the breast. *Invest Radiol*. 2005;40(7):412-420. https://doi.org/10.1097/01.rli.0000166940.72971.4a
14. Xu L, Lin Y, Xi ZN, Shen H, Gao PY. Magnetic resonance elastography of the human brain: a preliminary study. *Acta Radiol*. 2007;48(1):112-115. https://doi.org/10.1080/02841850601026401
15. Xu L, Lin Y, Han JC, Xi ZN, Shen H, Gao PY. Magnetic resonance elastography of brain tumors: preliminary results. *Acta Radiol*. 2007;48(3):327-330. https://doi.org/10.1080/02841850701199967
16. Murphy MC, Huston J, Jack CR, et al. Decreased brain stiffness in Alzheimer's disease determined by magnetic resonance elastography. *J Magn Reson Imaging*. 2011;34(3):494-498. https://doi.org/10.1002/jmri.22707

17. Romano A, Scheel M, Hirsch S, Braun J, Sack I. In vivo waveguide elastography of white matter tracts in the human brain. *Magn Reson Med*. 2012;68(5):1410-1422. https://doi.org/10.1002/mrm.24141
18. Murphy MC, Huston J, Glaser KJ, et al. Preoperative assessment of meningioma stiffness using magnetic resonance elastography. *J Neurosurg*. 2013;118(3):643-648. https://doi.org/10.3171/2012.9.JNS12519
19. Feng Y, Clayton EH, Chang Y, Okamoto RJ, Bayly PV. Viscoelastic properties of the ferret brain measured in vivo at multiple frequencies by magnetic resonance elastography. *J Biomech*. 2013;46(5):863-870. https://doi.org/10.1016/j.jbiomech.2012.12.024
20. Hatt A, Cheng S, Tan K, Sinkus R, Bilston LE. MR elastography can be used to measure brain stiffness changes as a result of altered cranial venous drainage during jugular compression. *Am J Neuroradiol*. 2015;36(10):1971-1977. https://doi.org/10.3174/ajnr.A4361
21. Arani A, Plewes D, Chopra R. Transurethral prostate magnetic resonance elastography: prospective imaging requirements. *Magn Reson Med*. 2011;65(2):340-349. https://doi.org/10.1002/mrm.22633
22. Sahebjavaher RS, Baghani A, Honarvar M, Sinkus R, Salcudean SE. Transperineal prostate MR elastography: initial in vivo results. *Magn Reson Med*. 2013;69(2):411-420. https://doi.org/10.1002/mrm.24268
23. Arani A, Da Rosa M, Ramsay E, Plewes DB, Haider MA, Chopra R. Incorporating endorectal MR elastography into multi-parametric MRI for prostate cancer imaging: initial feasibility in volunteers. *J Magn Reson Imaging*. 2013;38(5):1251-1260. https://doi.org/10.1002/jmri.24028
24. Sahebjavaher RS, Frew S, Bylinskii A, et al. Prostate MR elastography with transperineal electromagnetic actuation and a fast fractionally encoded steady-state gradient echo sequence. *NMR Biomed*. 2014;27(7):784-794. https://doi.org/10.1002/nbm.3118
25. Klatt D, Yasar TK, Royston TJ, Magin RL. Sample interval modulation for the simultaneous acquisition of displacement vector data in magnetic resonance elastography: theory and application. *Phys Med Biol*. 2013;58(24):8663-8675. https://doi.org/10.1088/0031-9155/58/24/8663
26. Yasar TK, Klatt D, Magin RL, Royston TJ. Selective spectral displacement projection for multifrequency MRE. *Phys Med Biol*. 2013;58(16):5771-5781. https://doi.org/10.1088/0031-9155/58/16/5771
27. Nir G, Sahebjavaher RS, Sinkus R, Salcudean SE. A framework for optimization-based design of motion encoding in magnetic resonance elastography. *Magn Reson Med*. 2015;73(4):1514-1525. https://doi.org/10.1002/mrm.25280
28. Guenthner C, Runge JH, Sinkus R, Kozerke S. Analysis and improvement of motion encoding in magnetic resonance elastography. *NMR Biomed*. 2018;31(5):e3908. https://doi.org/10.1002/nbm.3908
29. Rump J, Klatt D, Braun J, Warmuth C, Sack I. Fractional encoding of harmonic motions in MR elastography. *Magn Reson Med*. 2007;57(2):388-395. https://doi.org/10.1002/mrm.21152
30. Garteiser P, Sahebjavaher RS, Ter Beek LC, et al. Rapid acquisition of multifrequency, multislice and multidirectional MR elastography data with a fractionally encoded gradient echo sequence. *NMR Biomed*. 2013;26(10):1326-1335. https://doi.org/10.1002/nbm.2958
31. Maderwald S, Uffmann K, Galbán CJ, de Greiff A, Ladd ME. Accelerating MR elastography: a multiecho phase-contrast gradient-echo sequence. *J Magn Reson Imaging*. 2006;23(5):774-780. https://doi.org/10.1002/jmri.20570
32. Pruessmann KP, Weiger M, Scheidegger MB, Boesiger P. SENSE: sensitivity encoding for fast MRI. *Magn Reson Med*. 1999;42(5):952-962. https://doi.org/10.1002/(SICI)1522-2594(199911)42:5<952::AID-MRM16>3.0.CO;2-S
33. Runge J, Hoelzl S, Sudakova J, et al. A novel MR elastography transducer concept based on a rotational eccentric mass: the gravitational transducer. *Proc Int Soc Magn Reson Med*. 2017;25:1369.
34. Fovargue D, Kozerke S, Sinkus R, Nordsletten D. Robust MR elastography stiffness quantification using a localized divergence free finite element reconstruction. *Med Image Anal*. 2018;44:126-142. https://doi.org/10.1016/j.media.2017.12.005
35. Fehlner A, Hirsch S, Weygandt M, et al. Increasing the spatial resolution and sensitivity of magnetic resonance elastography by correcting for subject motion and susceptibility-induced image distortions. *J Magn Reson Imaging*. 2017;46(1):134-141. https://doi.org/10.1002/jmri.25516
36. Dittmann F, Reiter R, Guo J, et al. Tomoelastography of the prostate using multifrequency MR elastography and externally placed pressurized-air drivers. *Magn Reson Med*. 2018;79(3):1325-1333. https://doi.org/10.1002/mrm.26769

SUPPORTING INFORMATION

Additional supporting information may be found online in the Supporting Information section at the end of the article.

How to cite this article: Guenthner C, Sethi S, Troelstra M, Dokumaci AS, Sinkus R, Kozerke S. Ristretto MRE: A generalized multi-shot GRE-MRE sequence. *NMR in Biomedicine*. 2019;32:e4049. https://doi.org/10.1002/nbm.4049

APPENDIX

PROOF THAT N_D MUST BE A CO-PRIME OF N_P IN RISTRETTO MRE

In Equation 13, we state that the delay factor $N_D < N_P$ must be chosen from the set of co-primes of N_P. Let us assume that N_D is not a co-prime, i.e.

$$\exists a < N_P: \quad aN_D = \mathrm{LCM}(N_D, N_P) < N_D N_P. \tag{21}$$

Thus, a times application of the recurrence equation 12 determining the next acquired wave-phase index p_{n+1} leads to

$$p_{n+a} = (p_n + aN_D) \bmod N_P. \tag{22}$$

By construction $aN_D = \mathrm{LCM}(N_D, N_P)$ is divisible by N_P and can be cancelled. Hence,

$$\Leftrightarrow p_{n+a} = p_n. \tag{23}$$

Thus, the acquisition with a delay of N_D not being co-prime of N_P leads to the acquisition of only a subset of wave-phase offsets with exactly $a < N_P$ unique elements. Hence, N_D must be chosen such that $\mathrm{LCM}(N_D, N_P) \equiv N_D N_P$, i.e. N_D is a co-prime of N_P.